FEBS Letters 586 (2012) 2548–2554

journal homepage: www.FEBSLetters.org

Conformational dynamics of yeast calmodulin in the Ca^{2+}-bound state probed using NMR relaxation dispersion

Kenji Ogura [a,*], Hideyasu Okamura [b,c], Masato Katahira [b], Etsuko Katoh [c], Fuyuhiko Inagaki [a]

[a] Department of Structural Biology, Faculty of Advanced Life Science, Hokkaido University, Kita 21 Nishi 11, Sapporo 001-0021, Japan
[b] Bioenergy Research Section, Institute of Advanced Energy, Kyoto University, Gokasho, Uji, Kyoto 611-0011, Japan
[c] Biomolecular Research Unit, Agrogenomics Research Center, National Institute of Agrobiological Science, 2-1-2 Kannondai, Tsukuba, Ibaraki 305-8602, Japan

ARTICLE INFO

Article history:
Received 29 March 2012
Revised 31 May 2012
Accepted 19 June 2012
Available online 28 June 2012

Edited by Judit Ovádi

Keywords:
Calmodulin
NMR
Protein dynamics
Relaxation dispersion
Yeast

ABSTRACT

Most calmodulin (CaM) in apo and Ca^{2+}-bound states show a dumb-bell-like structure, involving the N- and C-terminal domains, connected with a flexible linker. However, Ca^{2+}-bound yeast calmodulin (yCaM) takes on a unique globular structure; the target-binding site of this protein is autoinhibited. We applied NMR relaxation dispersion experiments to yCaM in the Ca^{2+}-bound state. The amide ^{15}N and $^{1}H^{N}$ relaxation dispersion profiles indicated the presence of conformational dynamics for specific residues at the interface between the N- and C-terminal domains. We conclude that these conformational dynamics were derived from the mobility of the C-terminal domain.

1. Introduction

Calmodulin (CaM) is a Ca^{2+}-signaling protein that binds to a wide variety of target proteins in response to changes in intracellular Ca^{2+} levels. CaM consists of two globular domains, each comprising two EF-hand motifs and a flexible linker [1,2]. A pair of Ca^{2+}-binding sites is located on each globular domain. The EF-hand motifs are referred to as EF1, EF2, EF3, and EF4, numbered from the N-terminus; thus, CaM can bind a total of four Ca^{2+}-ions.

CaM is a highly conserved protein ubiquitously expressed in eukaryotic cells. The amino acid sequences of CaM isoforms from vertebrates, *Drosophila,* and scallops are nearly identical, with sequence identities of more than 90%. The amino acid sequence of the yeast *Saccharomyces cerevisiae* CaM (yCaM), however, shares only approximately 60% identity with vertebrate CaM. This sequence difference confers unique properties to yCaM. The most distinguishing characteristic of yCaM is the lack of Ca^{2+}affinity of the fourth EF-hand motif. Earlier work has shown that, because of the substitution of highly conserved Asp and Glu residues in EF4 of yCaM, EF4 lacks Ca^{2+}-binding ability, and hence, yCaM can bind only three Ca^{2+}-ions per molecule [3].

Recently, we have determined the solution structures of yCaM in the Ca^{2+}-bound form, as well as in a complex with a target peptide derived from calcineurin A1, by using nuclear magnetic resonance (NMR) spectroscopy [4]. In the Ca^{2+}-bound state, surprisingly, the EF1, EF2, and EF3 regions of yCaM showed a compact globular form, while the EF4 region presented a disordered conformation. The globular structure, consisting of the EF1, EF2, and EF3 regions, was confirmed by small angle X-ray scattering (SAXS) experiments, as well as by NMR spectral comparison of the full-length yCaM with an EF4-truncation mutant. The unique structure of the Ca^{2+}-bound yCaM, which retained the EF1, EF2, and EF3 regions, but not the EF4 region, is probably related to Ca^{2+}-mediated signal transduction in yeast. However, the functional consequences of the compact structure of the EF1–3 regions and the disordered conformation of the EF4 region of Ca^{2+}-bound yCaM are elusive.

Here, we describe an NMR relaxation dispersion study aimed at probing the conformational dynamics of Ca^{2+}-bound yCaM. NMR relaxation dispersion techniques are powerful tools for studying conformational dynamics or structural changes of proteins on microsecond–millisecond time-scales. Our NMR relaxation dispersion analyses of Ca^{2+}-bound yCaM and a mutant of this protein revealed the backbone conformational dynamics of residues in the EF1, EF2, and EF3 regions, especially those located in the interface between the N-terminal domain (EF1 and EF2) and the C-terminal domain (EF3). Moreover, we inferred structural properties for the EF3 region in its minor structural state by comparing the chemical shifts of amide ^{15}N and ^{1}H with those of the EF3 fragment in its Ca^{2+}-bound and free states.

* Corresponding author. Fax: +81 11 706 9012.
E-mail address: k-ogura@mail.sci.hokudai.ac.jp (K. Ogura).

0014-5793/$36.00
http://dx.doi.org/10.1016/j.febslet.2012.06.031

2. Materials and methods

2.1. Sample preparation

For NMR measurements, the EF4-deletion mutant of yCaM, comprising the regions of EF1–3 [referred to as yCaM(1–120)], was prepared as described previously [4]. Briefly, a uniformly ^{15}N, ^{2}H-labeled yCaM(1–120) protein, fused to a His_6 tag, was expressed in the *Escherichia coli* BL21 Star (DE3) strain (Life Technologies, Carlsbad, CA, USA) that was grown in MP medium containing $^{15}NH_4Cl$ (2 g/l), ^{2}H-labeled glucose (4 g/l), and $^{2}H_2O$ (99.8% atom of ^{2}H). yCaM(1–120) was purified using a Ni–NTA affinity resin (Qiagen, Hilden, Germany) and a Superdex75 gel-filtration column (GE Healthcare Life Sciences, Little Chalfont, UK), and concentrated to approximately 1.0 mM. A vector for expressing the yCaM(1–120) mutant containing the Leu18Cys and Leu109Cys amino acid substitutions (yCaM(1–120)L18C/L109C) was prepared using a QuikChange site-directed mutagenesis kit (Agilent Technologies, Santa Clara, CA, USA).

DNA encoding the yCaM(78–120) fragment, corresponding to the EF3 region, was cloned into a modified version of the pET21d (Merck, Darmstadt, Germany), creating a fusion protein consisting of an N-terminal His_6 tag followed by a GB1 domain, a PreScission Protease cleavage site, followed by yCaM(78–120). Proteins were expressed in *E. coli* BL21 Star (DE3) cells.

For the preparation of $^{13}C/^{15}N$-labeled proteins, cells were grown in MP medium containing $^{15}NH_4Cl$ (2 g/l) and ^{13}C-labeled glucose (4 g/l) at 37 °C. Protein expression was induced at an OD_{600} of 0.7 by the addition of isopropyl-1-thio-β-galactopyranoside to a final concentration of 0.1 mM, at 20 °C. The induced cells were cultured at 20 °C for 16 h. For preparation of yCaM(78–120) fragment, the disrupted cell lysate was subjected to affinity chromatography using a Ni–NTA resin. The eluted fractions were incubated for 12 h at 4 °C with PreScission Protease (GE Healthcare Life Sciences, Little Chalfont, UK) to cleave the fusion protein. His_6-tagged GB1 was then removed on a second Ni–NTA column. Finally, the isolated yCaM(78–120) was purified by gel filtration on a Superdex 75 column.

2.2. NMR relaxation dispersion measurements for Ca^{2+}-bound yCaM(1–120) and the mutant

The NMR samples were prepared in 20 mM MES–NaOH buffer (pH 6.5), 150 mM NaCl, and 10 mM $CaCl_2$ in 90% H_2O. Relaxation dispersion profiles of ^{15}N and $^{1}H^{N}$ were recorded using relaxation-compensated CPMG pulse sequences [5–7] at 25 °C (carefully corrected by the chemical shifts of ethylene glycol) on Varian Inova 800 and 600 NMR spectrometers equipped with room-temperature probes. Two-dimensional ^{1}H–^{15}N-correlated spectra were collected as a series of data sets with CPMG frequencies (ν_{CPMG}) of 50, 100, 150, 200, 250, 300, 400, 500, 600, 800, and 1000 Hz for ^{15}N, and 50, 100, 150, 200, 250, 350, 500, 750, 1000, 1250, 1500, and 2000 Hz for $^{1}H^{N}$, respectively. A constant-time relaxation delay T_{CP} was set to 40 ms for both experiments. Spectra were recorded as 200 × 600 complex points with a 2.5-s repetition delay and by using 8 scans for each increment. The total experimental time was 27 h for ^{15}N, and 29 h for $^{1}H^{N}$, respectively, on both 800 and 600 MHz spectrometers. Data sets were processed with the NMRPipe/nmrDraw program suit [8], and the peak intensities were quantified with the Sparky program [9]. The transverse relaxation rates $R_{2,\mathrm{eff}}$ for each of the ν_{CPMG} frequencies were calculated as $R_{2,\mathrm{eff}} = -\ln\left(I(\nu_{CPMG})/I_0\right)/T_{CP}$, where $I(\nu_{CPMG})$ is the peak intensity obtained for a given value of ν_{CPMG}, and I_0 is the peak intensity obtained when the CPMG block is omitted. The uncertainties, σ_I, associated with the peak intensities, were estimated using the standard deviation of the spectral noise. The uncertainties, σ_{R2}, for the R_2 rate constants were calculated as follows:

$$\sigma_{R2}(\nu_{CPMG}) = \frac{1}{T_{CP}}\left(\left(\frac{\sigma_{I_0}}{I_0}\right)^2 + \left(\frac{\sigma_{I(\nu_{CPMG})}}{I(\nu_{CPMG})}\right)^2\right)^{1/2}$$

2.3. Fitting calculation for relaxation dispersion data

^{15}N and $^{1}H^{N}$ relaxation data obtained for Ca^{2+}-bound yCaM(1–120) from the two static fields (18.8 and 14.1 T) were numerically fit by using an in-house program written in Mathematica 7, which has been described previously [10]. Briefly, the theoretical function $R_{2,calc}$ used to fit a two-state (A and B) exchange model, was as follows:

$$R_{2,calc} = -\frac{1}{2n\tau_{CP}}\ln\frac{M_A(2n\tau_{CP})}{M_A(0)},$$

where $T_{CP} = 2n\tau_{CP}$ with $2n$ refocusing pulses separated by delays of τ_{CP} within the T_{CP} period, the magnetization vector $\mathbf{M}(t) = (M_A(t), M_B(t))^T$, and $\mathbf{M}(2n\tau_{CP})$, with the evolution matrices $\mathbf{A}$ and $\mathbf{A}^*$ as

$$\mathbf{M}(2n\tau_{CP}) = \left(\exp\left(\frac{\mathbf{A}\tau_{CP}}{2}\right)\exp(\mathbf{A}^*\tau_{CP})\exp\left(\frac{\mathbf{A}\tau_{CP}}{2}\right)\right)^n\mathbf{M}(0)$$

and

$$\mathbf{A} = \begin{bmatrix} -R_{2A} - k_{AB} & k_{BA} \\ k_{AB} & -R_{2B} - k_{BA} + i\Delta\omega_{AB} \end{bmatrix}$$

$$\mathbf{A}^* = \begin{bmatrix} -R_{2A} - k_{AB} & k_{BA} \\ k_{AB} & -R_{2B} - k_{BA} - i\Delta\omega_{AB} \end{bmatrix},$$

where k_{AB} and k_{BA} are the rate constants for A to B and B to A transitions, respectively, $\Delta\omega$ is the frequency difference between the A and B states, and R_{2A} and R_{2B} are the transverse relaxation rate constants (assuming that $R_{2A} = R_{2B} = R_{20}$). The error function for the non-linear fits of R_{20}, k_{AB}, k_{BA}, and $\Delta\omega$ was

$$\chi^2 = \sum_{\nu_{CPMG}}\frac{\left(R_2(\nu_{CPMG}) - R_{2,calc}(\nu_{CPMG})\right)^2}{\sigma_{R2}(\nu_{CPMG})^2}.$$

Initially, data for 19 residues for ^{15}N (59 for $^{1}H^{N}$; out of data available for 102 residues) were selected based on the relatively large dispersion profiles of their relaxation curves. To determine the global kinetic parameters k_{ex} (=$k_{AB} + k_{BA}$) and P_a (=$k_{BA}/(k_{AB} + k_{BA})$), a cycle consisting of the selected residue-specific fits for $\Delta\omega$ and R_{20}, followed by a global fit for the kinetic parameters, was repeated until the total χ^2 value was reduced in size. Finally, the $\Delta\omega$ and R_{20} values for each of the 102 residues were fit, keeping the calculated kinetic parameters fixed. Errors associated with the parameters used in the fits were estimated by Monte Carlo simulations. The fitted chemical shift differences ($\Delta\omega_N$ and $\Delta\omega_H$), with errors and χ^2 values for each residue, are summarized in Supplemental Table S1.

To determine the signs of $\Delta\omega_H$, NMR measurements of relaxation dispersion for $^{15}N/^{2}H$-labeled Ca^{2+}-bound yCaM(1–120) were performed at 25 °C, using TROSY-based ^{1}H–^{15}N zero-quantum (ZQ) and double-quantum (DQ) CPMG pulse sequences [11] on a Varian Inova 600 NMR spectrometer. Two-dimensional ^{1}H–^{15}N-correlated spectra were collected as series of data sets with CPMG frequencies of 50, 100, 200, 300, 400, 500, 600, 800, and 1000 Hz for ZQ and DQ experiments. A constant-time relaxation delay, T_{CP}, was set to 40 ms. Spectra were recorded as 200 × 600 complex points, with a 2.5-s repetition delay and by using 8 scans for each increment. The total experimental time was 24 h for each coherent pathway.

2.4. NMR backbone resonance assignments for Ca^{2+}-bound yCaM(1–120) mutant and yCaM(78–120) fragment

NMR measurements for backbone $^{1}H^{N}$, ^{13}C, and ^{15}N resonance assignments of the Ca^{2+}-bound yCaM(1–120)L18C/L109C mutant and the yCaM(78–120) fragment were run on a Varian Inova 600 MHz NMR spectrometer at 25 °C and on a Varian Inova 500 MHz NMR spectrometer at 35 °C, respectively. The following experiments were run: 2D ^{1}H-^{15}N HSQC, 2D ^{1}H–^{13}C HSQC, 3D HNCO, 3D HN(CO)CA, 3D HNCA, 3D CBCA(CO)NH, 3D HNCACB, 3D HBHA(CBCACO)NH, and 3D HN(CA)HA. Spectral analysis and sequential assignments were performed with the Sparky and Paces [12] programs. The assigned chemical shifts of ^{15}N and $^{1}H^{N}$ for the apo and the Ca^{2+}-bound yCaM(78–120) fragment are summarized in Supplemental Table S2.

3. Results and discussion

3.1. Relaxation dispersion analysis of Ca^{2+}-bound yCaM

A uniformly ^{15}N- and ^{2}H-labeled sample of Ca^{2+}-bound yCaM(1–120) was subjected to ^{15}N and $^{1}H^{N}$ relaxation dispersion experiments. Fig. 1 shows the various curves of ^{15}N and $^{1}H^{N}$ dispersion profiles for Ca^{2+}-bound yCaM(1–120) recorded at static magnetic fields (18.8 and 14.1 T) and 25 °C. Significant dispersion for Val91, Phe92, Asp93, Lys94, Asn95, and Leu99 could be observed, whereas none was visible for Gly96 and Gly98. To extract exchange parameters, ^{15}N and $^{1}H^{N}$ relaxation dispersion data of 109 residues were separately fit to two-state exchange models, so that the global parameters k_{ex} and P_a could be extracted with absolute values of chemical shift differences between two states, $\Delta\omega_N$ and $\Delta\omega_H$, which are specific for each residue (Supplemental Table S1). The fits revealed an exchange process, at a rate of *ca.* 250 s^{-1} between two states, with 90% population of the major state (Table 1). Intriguingly, the exchange parameters, which were independently obtained from ^{15}N and $^{1}H^{N}$ dispersion data, showed similar values of k_{ex} and P_a. This result supported the validity of both the experiments and the analysis.

Table 1
^{15}N and $^{1}H^{N}$ exchange parameters for Ca^{2+}-bound yCaM(1–120) at 25 °C.

	k_{ex} (s^{-1})	P_a
^{15}N	247.577 ± 30.350	0.903 ± 0.007
$^{1}H^{N}$	278.682 ± 17.986	0.904 ± 0.004

To identify the residues exposed to conformational exchange on Ca^{2+}-bound yCaM(1–120), the values of normalized $\Delta\omega$, which is defined as $((\Delta\omega_N/5)^2 + (\Delta\omega_H)^2)^{1/2}$, were plotted as functions of the amino acid sequence in Fig. 2a. Whereas most normalized $\Delta\omega$ values were less than 0.2 ppm, the residues Phe16, Met72, Glu84, Asp93, Ala102, Leu105, His107, and Thr110, which are mainly located in the EF3 region, showed normalized $\Delta\omega$ values significantly larger than 0.25 ppm. Moreover, residues showing intermediate $\Delta\omega$ values (0.1–0.2 ppm) were distributed throughout the EF3 region, as well as in a small section of the EF1 region. Although $\Delta\omega$ values were not particularly large, this result showed that the EF3 region experiences relatively large conformational exchanges between the major and minor states than do the EF1 and EF2 regions of Ca^{2+}-bound yCaM(1–120). The $\Delta\omega$ values were mapped onto the previously reported structure of Ca^{2+}-bound yCaM(1–120) (Fig. 2b) [4]. This revealed that residues showing large $\Delta\omega$ values were localized on the interacting surface between the N-terminal domain (EF1 and EF2) and the EF3 region. This result suggested that the dynamic conformational exchange occurred around the EF3 region.

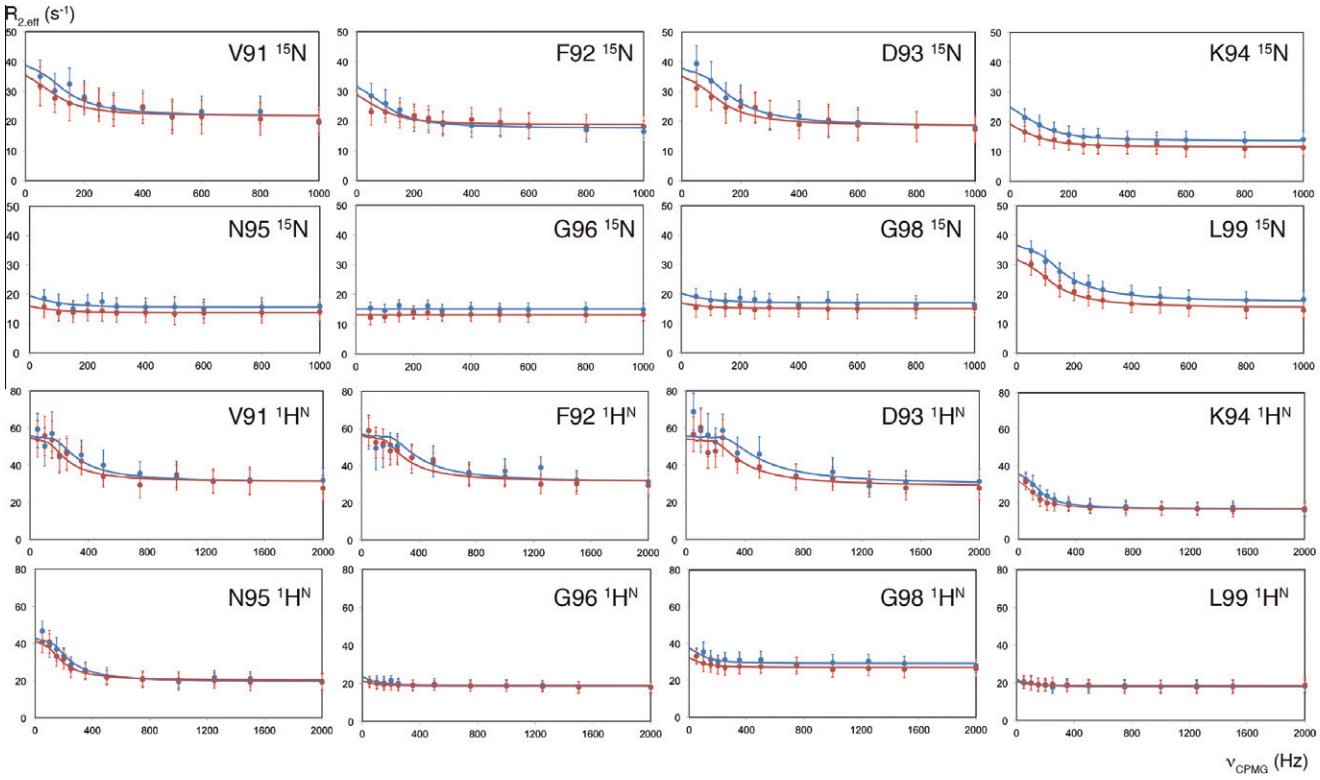

Fig. 1. Representative amide ^{15}N and $^{1}H^{N}$ single-quantum relaxation dispersion profiles from Val91 to Leu99 of Ca^{2+}-bound yCaM(1–120), recorded at a static magnetic field of 18.8 T (blue) and 14.1 T (red), are shown.

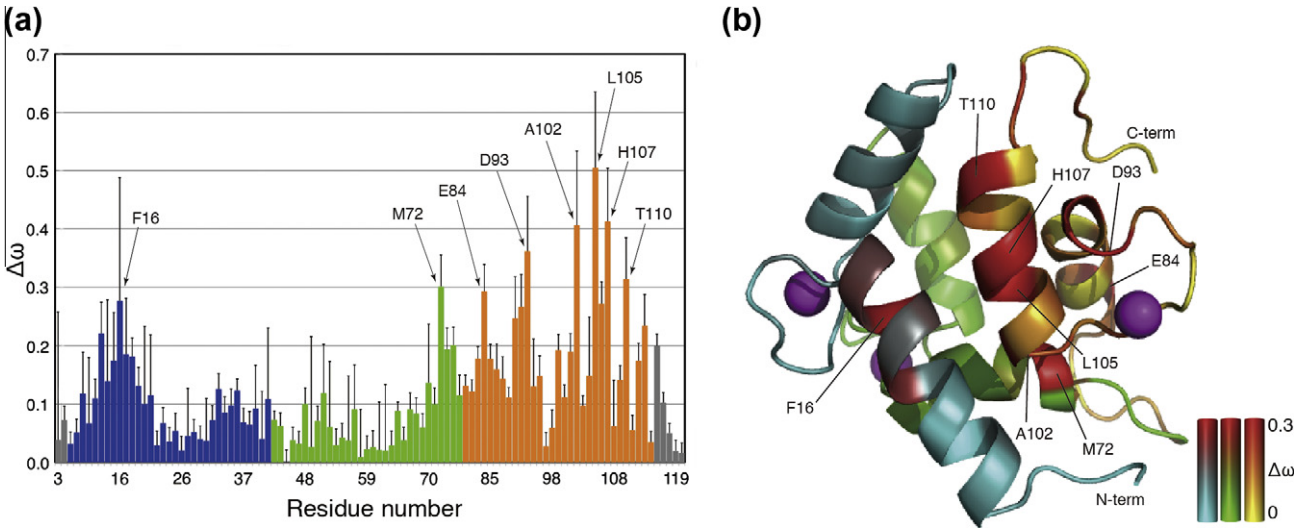

Fig. 2. (a) Normalized chemical shift differences plotted as functions of amino acid sequence for Ca^{2+}-bound yCaM(1–120), where values of normalized Δω is defined as $((\Delta\omega_N/5)^2 + (\Delta\omega_H)^2)^{1/2}$. The bars corresponding to residues in EF1 (residues 6–42), EF2 (residues 43–78), and EF3 (residues 79–115) are colored blue, green, and orange, respectively. Selected residues (Δω > 0.25 ppm) are indicated using the one-letter amino acid code. (b) Ribbon diagram depicting the chemical shift difference between the major and minor states in Ca^{2+}-bound yCaM(1–120). The EF1, EF2, and EF3 regions are colored cyan, green, and yellow, respectively. Calcium ions are colored magenta. Residues are indicated by color gradation according to values of Δω (0.3 ppm as red, and basal color corresponding to no change in chemical shift). Selected residues (Δω > 0.25 ppm) are indicated using the one-letter amino acid code. The structure was drawn using PyMol (http://www.pymol.org).

3.2. Verification of the conformational exchange using a disulfide mutant

To verify that the conformational exchange involved the EF3 region, we generated a disulfide mutant, in which the orientation of the EF3 region toward the EF1–2 regions was fixed. Based on the NMR structure of the Ca^{2+}-bound yCaM(1–120) [4], we chose residues Leu18 and Leu109 as the mutational candidates. The distance of 4.6 Å between the Cβ atoms of these leucine residues was sufficient to allow formation of a disulfide bond when cysteine residues were used to replace both leucine residues (Fig. 3a). The ^{15}N-labeled yCaM(1–120)L18C/L109C mutant was thus prepared and

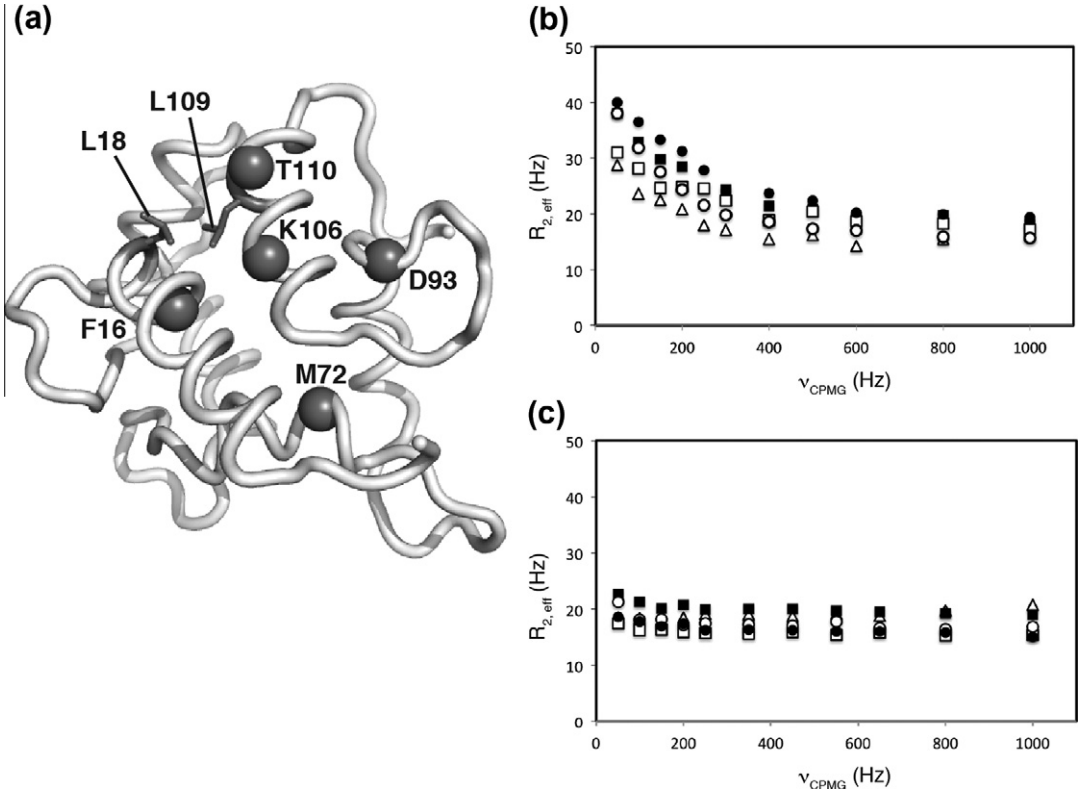

Fig. 3. (a) Cartoon diagram of Ca^{2+}-bound yCaM(1–120). Side chain atoms of mutational candidates, Leu18 and Leu109, are represented using a stick model. Amide nitrogen atoms of Phe16, Met72, Asp93, Lys106, and Thr110, showing relatively large relaxation dispersion profiles, are represented using a sphere model. In (b) and (c), ^{15}N relaxation profiles of residues Phe16 (△), Met72 (■), Asp93 (□), Lys106 (○), and Thr110 (●) (b) for Ca^{2+}-bound yCaM(1–120) and (c) for the Ca^{2+}-bound yCaM(1–120)L18C/L109C mutant are plotted.

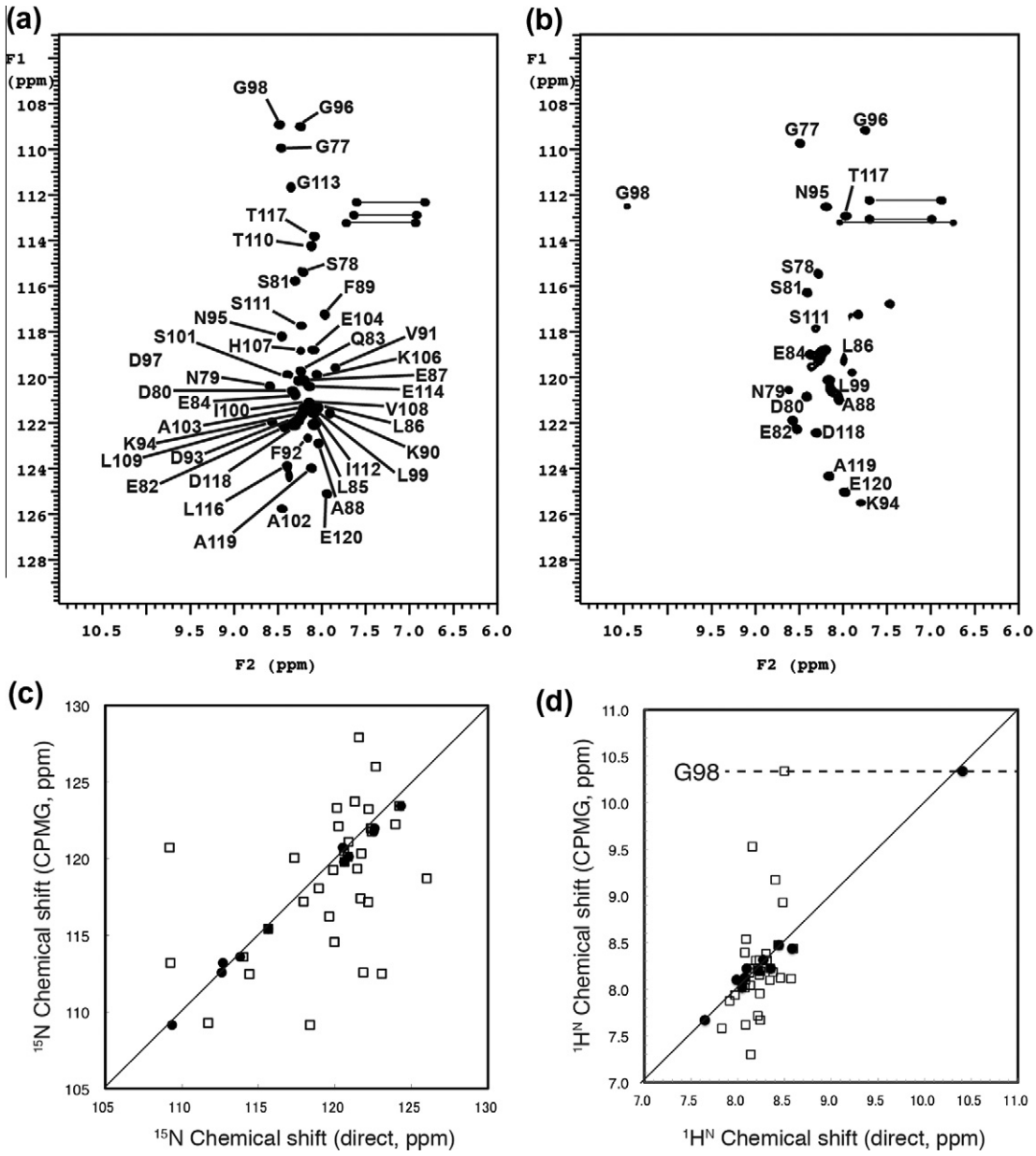

Fig. 4. ^{1}H–^{15}N HSQC spectra of the yCaM(78–120) fragment in the (a) apo and (b) Ca^{2+}-bound forms. Peaks of the main chain amide are labeled with their assignments. (c and d) Correlations between chemical shifts of the minor state, which were obtained from the relaxation dispersion data of Ca^{2+}-bound yCaM(1–120), and directly observed chemical shifts of the yCaM(78–120) fragment in apo (□) and Ca^{2+}-bound (●) forms for ^{15}N and $^{1}H^{N}$, respectively. In (d), the $^{1}H^{N}$ chemical shift of Gly98, obtained using CPMG experiments, is indicated by a broken line.

subjected to ^{15}N relaxation dispersion experiments. Formation of the disulfide bond between Cys18 and Cys109 was confirmed by the chemical shifts of the Cβ atoms (41.6 and 41.9 ppm, respectively); there were no other cysteine residues in the yCaM(1–120).

Fig. 3b shows the ^{15}N relaxation dispersion profiles of the Ca^{2+}-bound yCaM(1–120) for residues Phe16, Met72, Asp93, Lys106, and Thr110. As described previously, these residues showed significant dispersion curves and large Δω values between the major and minor states of the Ca^{2+}-bound yCaM(1–120) (Fig. 3b). On the other hand, introducing the disulfide bond in the L18C/L109C mutant changed the dispersion curves into flat profiles (Fig. 3c). Fig. 3b and c clearly demonstrate that the minor state of the Ca^{2+}-bound yCaM(1–120) disappears when a disulfide bond is introduced between the EF1 and EF3 regions. This finding indicates that the conformational exchange of the Ca^{2+}-bound yCaM(1–120) derives from the displacement of the EF3 region on the interacting surface of the N-terminal domain (EF1–2 regions). In the activated state of yCaM, the autoinhibition of the N-terminal domain, which is maintained by the EF3 region, must be released when a target-peptide approaches the interaction site on yCaM. Therefore, the EF3 region of Ca^{2+}-bound yCaM takes on a transient, rather than a rigid structure.

3.3. Inferring the structural properties of EF3 region in the minor state

To infer the structural properties of the EF3 region in the minor state, we compared the ^{15}N and $^{1}H^{N}$ chemical shifts obtained during the CPMG experiments and the directly measured values of the EF3 region in the Ca^{2+}-free (apo) state and Ca^{2+}-bound state. Although the apo yCaM(1–120) would have been preferable for chemical shift comparison, this protein aggregated extensively in the concentration range used for NMR experiments. Therefore,

we used the yCaM(78–120) fragment for comparison of chemical shift values.

First, the signs of $\Delta\omega_N$ for residues 78–120 in Ca^{2+}-bound yCaM(1–120) were obtained by comparing the peak positions of the major state in a pair of HSQC/HMQC spectra recorded at 18.8 T, based on the premise that the peak of the major state in a HSQC is slightly shifted to the position of the minor state in a HMQC spectrum [13]. Additionally, information about the signs of $\Delta\omega_H$ for the residues 78–120 of Ca^{2+}-bound yCaM(1–120) was also obtained by comparing the dispersion profiles of ^1H–^{15}N ZQ and DQ CPMG experiments. Since the signs of $\Delta\omega_N$ were known, we could obtain the signs of $\Delta\omega_H$ by using the relationship between the relative intensities of the ZQ and DQ dispersion profiles and the relative signs of $\Delta\omega_N{\cdot}\Delta\omega_H$ [14]. The signs of $\Delta\omega_N$ and $\Delta\omega_H$ for the residues 78–120 of Ca^{2+}-bound yCaM(1–120) are summarized in Supplemental Table S1.

Second, we assigned the backbone resonances for both the apo and the Ca^{2+}-bound yCaM(78–120) fragment, by using a suit of standard triple resonance NMR experiments (Fig. 4 and Supplemental Table S2). As shown in Fig. 4a, all amide signals of ^1H–^{15}N HSQC spectrum for yCaM(78–120) fragment in apo form were not well dispersed and were localized within a range of 7.8–8.6 ppm in the ^1H dimension. This result indicated that the yCaM(78–120) fragment does not take on a specific secondary structure, but rather has a disordered conformation. Moreover, this is consistent with the concept that an isolated EF-hand motif cannot maintain a folded structure.

In the presence of Ca^{2+} ions, on the other hand, we could assign only 25 residues out of 43 residues, because of the disappearance of many amide signals. This phenomenon occurred due to a structural exchange of the EF-hand motif on an intermediate time-scale. However, Gly98, which is located on the loop region connecting the two α-helices that comprise the EF-hand motif, showed a markedly large low-field shift in the presence of Ca^{2+} ions. In early studies of CaM using NMR spectroscopy, such a low-field shift of the glycine residue, located on the Ca^{2+}-binding loop, was utilized to assess whether the EF-hand binds a Ca^{2+} ion [15,16]. Similarly, we concluded that the observed peaks of the yCaM(78–120) fragment in the presence of Ca^{2+} ions represented the protein in the Ca^{2+}-bound state.

Finally, we compared the ^{15}N and $^1H^N$ chemical shifts obtained using the CPMG experiments and the directly measured values of the EF3 region (Fig. 4c and d). Correlation plots of chemical shifts for the yCaM(78–120) fragment in the apo and Ca^{2+}-bound states versus the chemical shifts obtained using the CPMG experiments indicated that the chemical shift values of the minor state were more similar to those of the Ca^{2+}-bound states than to those of the apo state (i.e., disordered conformation). Correlation coefficients of the plots for ^{15}N ($^1H^N$) chemical shifts were 0.97 (0.92) for Ca^{2+}-bound yCaM(1–120). These values suggested that the EF3 region in the minor state retains the Ca^{2+}-bound form rather than apo form.

This hypothesis regarding Ca^{2+}-binding by the EF3 region in the minor state is supported by the fact that the $^1H^N$ chemical shifts of Gly98 (Fig. 4d) for the minor state (10.34 ppm) are very close to that for the major state (10.30 ppm), or for the Ca^{2+}-bound fragment (10.44 ppm), and are very different to that for the apo fragment (8.50 ppm; see Supplemental Tables S1 and S2). Moreover, by fitting the data derived from the ^{15}N and $^1H^N$ CPMG experiments, k_{ex} between the two states was determined to be *ca.* 250 s^{-1}. The off-rates of Ca^{2+} ions from vertebrate CaM molecules, which have been experimentally investigated by various methods, is known to be 10 s^{-1} for the high-affinity sites, and 500 s^{-1} for the low-affinity sites [17,18]. For yCaM, however, the off-rates of Ca^{2+} have not been reported. From the present study, since the EF3 region in the minor form results neither in release of the Ca^{2+} ions, nor in unfolding to a disordered conformation, the off-rate of Ca^{2+} for the EF3 region was estimated as being less than 250 s^{-1}. Since the exchange rate, k_{ex}, is higher than the off-rate of the Ca^{2+} ion, once the Ca^{2+}-bound yCaM changes conformation into the minor state, the EF3 region will retain the Ca^{2+}-bound form until the yCaM returns to the major state.

4. Conclusion

We investigated the conformational dynamics of Ca^{2+}-bound yCaM using NMR relaxation dispersion methods. Our relaxation dispersion experiments revealed the existence of a minor structural state (~10%) and the exchange rate (~250 s^{-1}) for Ca^{2+}-bound yCaM. The structural exchange around the EF3 region was verified by a mutational study making use of a disulfide bond-mutant. Comparing the chemical shift values obtained using relaxation dispersion with those derived by direct measurements revealed that the EF3 region maintains the folded structure in the Ca^{2+}-bound form.

In the major state, Ca^{2+}-bound yCaM has a compact globular form; therefore, the target-binding site is autoinhibited by the EF3 region. Such an autoinhibitory structure is a unique characteristic of yCaM; however, it seems energetically unfavorable for target recognition. If Ca^{2+}-bound yCaM maintained a rigid, closed form at all times, the target peptide would not be able to approach the interaction site on yCaM because of the steric hindrance presented by the EF3 region. The present study suggests that the conformational change between the major and minor states involves a structural transition from the compact, "closed" form (major state) to the "open" form (minor state) of the EF3 region. This proposal is supported by the fact that the interacting surface between the N-terminal domain and the EF3 region must be opened when yCaM binds the target-peptide for yCaM. Thus, the presence of the minor, "open" form of Ca^{2+}-bound yCaM is consistent with the molecular function of yCaM. Further investigations, such as residual dipolar coupling measurements combined with relaxation dispersion experiments, are required to conclusively prove whether the minor state of the EF3 region is in an open conformation or not.

Acknowledgements

K.O. was supported by Grant-in-Aid for Scientific Research from JSPS (22570109) and MEXT (24121701). M.K. was supported by grants from MEXT(21370047, 22121517, and 23657072), JST (SENTAN and CREST), the Sumitomo-Denko Foundation, and the Iwatani Foundation.

Appendix A. Supplementary data

Supplementary data associated with this article can be found, in the online version, at http://dx.doi.org/10.1016/j.febslet.2012.06.031.

References

[1] Babu, Y.S., Sack, J.S., Greenhough, T.J., Bugg, C.E., Means, A.R. and Cook, W.J. (1985) Three-dimensional structure of calmodulin. Nature 315, 37–40.
[2] Barbato, G., Ikura, M., Kay, L.E., Pastor, R.W. and Bax, A. (1992) Backbone dynamics of calmodulin studied by ^{15}N relaxation using inverse detected two-dimensional NMR spectroscopy: the central helix is flexible. Biochemistry 31, 5269–5278.
[3] Matsuura, I., Ishihara, K., Nakai, Y., Yazawa, M., Toda, H. and Yagi, K. (1991) A site-directed mutagenesis study of yeast calmodulin. J Biochem 109, 190–197.
[4] Ogura, K., Kumeta, H., Takahasi, K., Kobashigawa, Y., Yoshida, R., Itoh, H., Yazawa, M. and Inagaki, F. (2012) Solution structures of yeast *Saccharomyces cerevisiae* calmodulin in calcium- and target peptide-bound states reveal similarities and differences to vertebrate calmodulin. Genes Cells 17, 159–172.

[5] Loria, P., Rance, M. and Palmer III, A.G. (1999) A relaxation-compensated Carr-Purcell-Meiboom-Gill sequence for characterizing chemical exchange by NMR spectroscopy. J. Am. Chem. Soc. 121, 2331–2332.
[6] Hansen, D.F., Pramodh, V., Lewis, E. and Kay, L.E. (2008) An improved ^{15}N relaxation dispersion experiment for the measurement of millisecond time-scale dynamics in proteins. J. Phys. Chem. B 112, 5898–5904.
[7] Ishima, R. and Torchia, D.A. (2003) Extending the range of amide proton relaxation dispersion experiments in proteins using a constant-time relaxation-compensated CPMG approach. J. Biomol. NMR 25, 243–248.
[8] Delaglio, F., Grzesiek, S., Vuister, G.W., Zhu, G., Pfeifer, J. and Bax, A. (1995) NMRPipe: a multidimensional spectral processing system based on UNIX pipes. J. Biomol. NMR 6, 277–293.
[9] Goddard TD, Kneller DG. SPARKY 3, University of California, San Francisco.
[10] Okamura, H., Nishikiori, M., Xiang, H., Ishikawa, M. and Katoh, E. (2011) Interconversion of two GDP-bound conformations and their selection in an Arf-family small G protein. Structure 19, 988–998.
[11] Orekhov, V.Y., Korzhnev, D.M. and Kay, L.E. (2004) Double- and zero-quantum NMR relaxation dispersion experiments sampling millisecond time scale dynamics in proteins. J. Am. Chem. Soc. 126, 1886–1891.
[12] Coggins, B.E. and Zhou, P. (2003) PACES: Protein sequential assignment by computer-assisted exhaustive search. J. Biomol. NMR 26, 93–111.
[13] Skrynnikov, N.R., Dahlquist, F.W. and Kay, L.E. (2002) Reconstructing NMR spectra of "invisible" excited protein states using HSQC and HMQC experiments. J. Am. Chem. Soc. 124, 12352–12360.
[14] Korzhnev, D.M., Neudecker, P., Mittermaier, A., Orekhov, V.Y. and Kay, L.E. (2005) Multiple-site exchange in proteins studied with a suite of six NMR relaxation dispersion experiments: an application to the folding of a Fyn SH3 domain mutant. J. Am. Chem. Soc. 127, 15602–15611.
[15] Ikura, M., Minowa, O. and Hikichi, K. (1985) Hydrogen bonding in the carboxyl-terminal half-fragment 78–148 of calmodulin as studied by two-dimensional nuclear magnetic resonance. Biochemistry 24, 4264–4269.
[16] Ikura, M., Minowa, O., Yazawa, M., Yagi, K. and Hikichi, K. (1987) Sequence-specific assignments of downfield-shifted amide proton resonances of calmodulin. Use of two-dimensional NMR analysis of its tryptic fragments. FEBS Lett. 219, 17–21.
[17] Bayley, P., Ahlström, P., Martin, S.R. and Forsen, S. (1984) The kinetics of calcium binding to calmodulin: Quin 2 and ANS stopped-flow fluorescence studies. Biochem. Biophys. Res. Commun. 120, 185–191.
[18] Park, H.Y., Kim, S.A., Korlach, J., Rhoades, E., Kwok, L.W., Zipfel, W.R., Waxham, M.N., Webb, W.W. and Pollack, L. (2008) Conformational changes of calmodulin upon Ca^{2+} binding studied with a microfluidic mixer. Proc. Natl. Acad. Sci. U S A 105, 542–547.